Quantification of entanglement and coherence with purity detection

npj | quantum information

Article

Published in partnership with The University of New South Wales

https://doi.org/10.1038/s41534-024-00857-2

Quantification of entanglement and coherence with purity detection

Check for updates

Ting Zhang[1], Graeme Smith[2,3,4], John A. Smolin[5], Lu Liu[1], Xu-Jie Peng[1], Qi Zhao[6], Davide Girolami[7], Xiongfeng Ma[8], Xiao Yuan[9,10] & He Lu[1,11]

Entanglement and coherence are fundamental properties of quantum systems, promising to power near-future quantum technologies, such as quantum computation, quantum communication, and quantum metrology. Yet, their quantification, rather than mere detection, generally requires reconstructing the spectrum of quantum states, i.e., experimentally challenging measurement sets that increase exponentially with the system size. Here, we demonstrate quantitative bounds to operationally useful entanglement and coherence that are universally valid, analytically computable, and experimentally friendly. Specifically, our main theoretical results are lower and upper bounds to the coherent information and the relative entropy of coherence in terms of local and global purities of quantum states. To validate our proposal, we experimentally implement two purity detection methods in an optical system: shadow estimation with random measurements and collective measurements on pairs of state copies. The experiment shows that both the coherent information and the relative entropy of coherence of pure and mixed unknown quantum states can be bounded by purity functions. Our research offers an efficient means of verifying large-scale quantum information processing.

Entanglement is a fundamental trait of many-body quantum systems and a key resource for quantum information processing[1–5]. Recently, theoretical methods to characterize quantum superpositions have been generalized to evaluate quantum coherence in single systems[6] and explore its uses for quantum technologies[7–15]. Quantification of such resources provides insights on the true computational power of quantum devices[16–20], and many important measures are defined in terms of the von Neumann entropy $S(\rho) = -\mathrm{Tr}(\rho \log \rho)$. Besides, the von Neumann entropy has been found widespread applications in quantum date compression[21], quantum thermodynamics[22], capacity bounds for quantum channels[23] and many-body physics, from the characterization of topological matter[24–26], to dynamics out of equilibrium[27], to the understanding of tensor network methods[28] (see ref. 29 for a review). However, the quantification of von Neumann entropy is hard both theoretically and experimentally, as it necessitates knowledge of the full spectrum of the system state ρ. Clever methods that enable *witness* entanglement and coherence employ randomized measurements[30–33] and collective detections on many copies of quantum states to extract spectrum polynomials, e.g., the state purity $\mathrm{Tr}(\rho^2)$[34–39]. Yet, these protocols cannot be easily applied to *quantify* entanglement and coherence: there are no measures of quantum resources that can be expressed in terms of directly observable (polynomial) quantities.

In this letter, we address this challenge by proposing an efficient approach to identify quantitative bounds to entanglement and coherence of unknown quantum states in terms of purity functions, in contrast to other protocols based on local measurements[40,41]. We focus on the coherent information and relative entropy of coherence, which are both defined in terms of the von Neumann entropy and are information measures with compelling operational interpretations. The coherent information is related to the distillable entanglement and the capacity of quantum channels with applications in quantum communication, one-way entanglement distillation, quantum state merging, and quantum many-body physics[30,42–47]. The relative entropy of coherence lower bounds the distillable coherence and plays an important role in quantum thermodynamics, quantum metrology, quantum computing, quantum random number generation and quantum

[1]School of Physics, State Key Laboratory of Crystal Materials, Shandong University, Jinan 250100, China. [2]JILA, University of Colorado/NIST, 440 UCB, Boulder, CO 80309, USA. [3]Center for Theory of Quantum Matter, University of Colorado, Boulder, CO 80309, USA. [4]Department of Physics, University of Colorado, 390 UCB, Boulder, CO 80309, USA. [5]IBM T.J. Watson Research Center, 1101 Kitchawan Road, Yorktown Heights, NY 10598, USA. [6]QICI Quantum Information and Computation Initiative, Department of Computer Science, The University of Hong Kong, Pokfulam Road, Hong Kong, Hong Kong. [7]DISAT, Politecnico di Torino, Corso Duca degli Abruzzi 24, Torino 10129, Italy. [8]Center for Quantum Information, Institute for Interdisciplinary Information Sciences, Tsinghua University, Beijing 100084, China. [9]Center on Frontiers of Computing Studies, Peking University, Beijing 100871, China. [10]School of Computer Science, Peking University, Beijing 100871, China. [11]Shenzhen Research Institute of Shandong University, Shenzhen 518057, China. e-mail: xiaoyuan@pku.edu.cn; luhe@sdu.edu.cn

phase transitions[6,48,49]. We prove analytical upper and lower bounds on the coherent information and relative entropy of coherence of arbitrary finite-dimensional quantum states in terms of their local and global purities, which are measurable without spectrum reconstruction[50]. Then, we experimentally demonstrate our proposal in an optical system by implementing the randomized measurements scheme on four-qubit states, and collective measurements on two copies of two-qubit states. The experiment results confirm that operationally useful entanglement and coherence of unknown quantum states can be quantified without spectrum reconstruction.

Results

Our study has two main merits. First, it discovers simple analytical functions that quantify, rather than only witness, key quantum resources in arbitrary systems of finite dimension. Second, it shows an experimental comparison between the well-established interference-based method for non-tomographic exploration of quantum properties[51–54], and the recently introduced "shadow estimation" techniques[55–58]. Together, our study provides a theoretically universal and practically efficient means to benchmark features of unknown quantum systems.

Quantification of coherent information

For quantum states $\rho_{AB} \in \mathcal{H}_{d_A} \otimes \mathcal{H}_{d_B}$, the coherent information is defined by

$$I(A\rangle B) = S(\rho_B) - S(\rho_{AB}), \tag{1}$$

where A and B are subsystems and $\rho_B = \mathrm{Tr}_A(\rho_{AB})$ is the reduced density matrix on subsystem B. A positive value of $I(A\rangle B)$ signals operationally useful entanglement between subsystems A and B[46].

Measuring $I(A\rangle B)$ requires knowledge of the eigenvalues of the density matrices. We propose a method to obtain upper and lower bounds on the von Neumann entropy in terms of the global and marginal purity of the state. Given the spectral decomposition of a d-dimensional quantum state, i.e., $\rho = \sum_{i=1}^{d} \lambda_{i,\rho}|\psi_i\rangle\langle\psi_i|, \sum_i \lambda_{i,\rho} = 1, \langle\psi_i|\psi_j\rangle = \delta_{ij}, \lambda_{1,\rho} \geq \lambda_{2,\rho} \geq \ldots \lambda_{d,\rho}$, we determine the extreme values of the state entropy $S(\rho) = -\sum_{i=1}^{d} \lambda_{i,\rho}\log\lambda_{i,\rho}$ at fixed purity $\mathcal{P}(\rho) := \sum_{i=1}^{d}\lambda_{i,\rho}^2$, where the logarithm is written in base 2[59]. The spectrum $\{\lambda_{i,\rho}^{\mathrm{M}}\}$ that maximizes $S(\rho)$ is $\lambda_{1,\rho}^{\mathrm{M}} = \frac{1}{d} + \sqrt{\frac{d-1}{d}\left(\mathcal{P}(\rho) - \frac{1}{d}\right)}, \lambda_{2,\rho}^{\mathrm{M}} = \cdots = \lambda_{d,\rho}^{\mathrm{M}} = \frac{1-\lambda_{1,\rho}^{\mathrm{M}}}{d-1}$. The spectrum $\{\lambda_{i,\rho}^{\mathrm{m}}\}$ that minimizes $S(\rho)$ is given by $\lambda_{1,\rho}^{\mathrm{m}} = \lambda_{2,\rho}^{\mathrm{m}} = \cdots = \lambda_{k_\rho-1,\rho}^{\mathrm{m}} = \frac{1-\alpha_\rho}{k_\rho-1}, \lambda_{k_\rho,\rho}^{\mathrm{m}} = \alpha_\rho, \lambda_{k_\rho+1,\rho}^{\mathrm{m}} = \cdots = \lambda_{d,\rho}^{\mathrm{m}} = 0$, where $\alpha_\rho = 1/k_\rho - \sqrt{(1-1/k_\rho)(\mathcal{P}(\rho) - 1/k_\rho)}$ and k_ρ is the integer such that $\frac{1}{k_\rho} \leq \mathcal{P}(\rho) < \frac{1}{k_\rho - 1}$. We can immediately use these results to bound the coherent information as follows (see Supplementary Note 1 for details).

Result 1—Given a quantum state ρ_{AB}, its coherent information $I(A\rangle B)$ is bounded as follows:

$$l_e(\rho_{AB}) \leq I(A\rangle B) \leq u_e(\rho_{AB}) \tag{2}$$

where

$$\begin{aligned} l_e(\rho_{AB}) &= (\lambda_{k_{\rho_B},\rho_B}^{\mathrm{m}} - 1)\log\lambda_{1,\rho_B}^{\mathrm{m}} - \lambda_{k_{\rho_B},\rho_B}^{\mathrm{m}}\log\lambda_{k_{\rho_B},\rho_B}^{\mathrm{m}} \\ &\quad + (1-\lambda_{1,\rho_{AB}}^{\mathrm{M}})\log\frac{(1-\lambda_{1,\rho_{AB}}^{\mathrm{M}})}{(d-1)} + \lambda_{1,\rho_{AB}}^{\mathrm{M}}\log\lambda_{1,\rho_{AB}}^{\mathrm{M}}, \\ u_e(\rho_{AB}) &= (1-\lambda_{k_{\rho_{AB}},\rho_{AB}}^{\mathrm{m}})\log\lambda_{1,\rho_{AB}}^{\mathrm{m}} + \lambda_{k_{\rho_{AB}},\rho_{AB}}^{\mathrm{m}}\log\lambda_{k_{\rho_{AB}},\rho_{AB}}^{\mathrm{m}} \\ &\quad - (1-\lambda_{1,\rho_B}^{\mathrm{M}})\log\frac{(1-\lambda_{1,\rho_B}^{\mathrm{M}})}{(d_B-1)} - \lambda_{1,\rho_B}^{\mathrm{M}}\log\lambda_{1,\rho_B}^{\mathrm{M}}. \end{aligned} \tag{3}$$

The lower and upper bounds is tight for pure states ($\mathcal{P}(\rho_{AB}) = 1$) with $\mathcal{P}(\rho_B) = \frac{1}{d_B}$ and the difference $\epsilon_e = \mathcal{P}(\rho_B) - 1/d_B$ certifies the tightness of $u_e(\rho)$ and $l_e(\rho)$.

Quantification of quantum coherence

In a way similar to how non-factorizable superpositions of multipartite states, e.g. $\sum_i c_i|ii\ldots i\rangle$, yield entanglement, the quantumness of a system can be identified with the degree of coherence of its state $|\psi\rangle = \sum_i c_i|i\rangle, \sum_i |c_i|^2 = 1$, in a reference basis $\{|i\rangle\}$. One natural way to quantify the coherence of a state in a reference basis $\{|1\rangle, |2\rangle, \ldots, |d\rangle\}$ of a d-dimensional Hilbert space $\mathcal{H}_d$ is by measuring how far it is from the set of incoherent states $\mathcal{I}$[60,61]. The choice of distance function is, in principle, arbitrary. Yet, an important operational interpretation is enjoyed by the relative entropy of coherence[60]

$$C_{\mathrm{RE}}(\rho) = \min_{\sigma\in\mathcal{I}} S(\rho||\sigma) = S(\rho_d) - S(\rho), \tag{4}$$

where $\rho_d = \sum_i |i\rangle\langle i|\rho|i\rangle\langle i|$ is the state after dephasing in the reference basis. The the asymptotic limit of infinite system preparations, $C_{\mathrm{RE}}(\rho)$ represents the maximal rate of extraction of maximally coherent qubit states $1/2\sum_{i,j=0,1}|i\rangle\langle j|$ from ρ by incoherent operations. Like the coherent information, this quantity is bounded by the purity function (see Supplementary Note 1 for details).

Result 2—The relative entropy of coherence $C_{\mathrm{RE}}(\rho)$ is bounded as follows:

$$l_c(\rho) \leq C_{\mathrm{RE}}(\rho) \leq u_c(\rho), \tag{5}$$

where

$$\begin{aligned} l_c(\rho) &= (\lambda_{k_{\rho_d},\rho_d}^{\mathrm{m}} - 1)\log\lambda_{1,\rho_d}^{\mathrm{m}} - \lambda_{k_{\rho_d},\rho_d}^{\mathrm{m}}\log\lambda_{k_{\rho_d},\rho_d}^{\mathrm{m}} \\ &\quad + (1-\lambda_{1,\rho}^{\mathrm{M}})\log\frac{(1-\lambda_{1,\rho}^{\mathrm{M}})}{(d-1)} + \lambda_{1,\rho}^{\mathrm{M}}\log\lambda_{1,\rho}^{\mathrm{M}}, \\ u_c(\rho) &= (1-\lambda_{k_\rho,\rho}^{\mathrm{m}})\log\lambda_{1,\rho}^{\mathrm{m}} + \lambda_{k_\rho,\rho}^{\mathrm{m}}\log\lambda_{k_\rho,\rho}^{\mathrm{m}} \\ &\quad - (1-\lambda_{1,\rho_d}^{\mathrm{M}})\log\frac{(1-\lambda_{1,\rho_d}^{\mathrm{M}})}{(d-1)} - \lambda_{1,\rho_d}^{\mathrm{M}}\log\lambda_{1,\rho_d}^{\mathrm{M}}. \end{aligned} \tag{6}$$

This inequality chain, like the one in Eq. (2), is tight for pure states ($\mathcal{P}(\rho) = 1$) with a diagonal matrix of $\rho_d = \frac{1}{d}\mathbb{I}_d$ ($\mathcal{P}(\rho_d) = \frac{1}{d}$). The difference $\epsilon_c = \mathcal{P}(\rho_d) - 1/d$ certifies the tightness of $u_c(\rho)$ and $l_c(\rho)$. $\epsilon_e(\epsilon_c)\to 0$ indicates the maximally entangled state (maximally coherent state), which is of particular interest in quantum information science.

Detecting purity with shadow estimation

We first use shadow tomography [55,62,63] to detect the purity of the four-qubit biased Greenberger-Horne-Zeilinger (GHZ) states in the form of

$$|\mathrm{GHZ}_\theta\rangle = \cos\theta|HhHh\rangle_{11'22'} + \sin\theta|VvVv\rangle_{11'22'}, \tag{7}$$

which are encoded on the polarization and path degrees of freedom (DOF) of photons. As shown in Fig. 1a, the polarization-entangled photons are generated from a periodically poled potassium titanyl phosphate (PPKTP) crystal set at Sagnac interferometer. Then, we then sent two photons into two beam displacers (BDs) as shown in Fig. 1b, which transmits the vertical polarization and deviates from the horizontal polarization. Consequently, the biased GHZ state $|\mathrm{GHZ}_\theta\rangle$ is obtained, where h (v) denotes the deviated (transmitted) spatial mode.

We prepare eleven $\rho_{\mathrm{GHZ}_\theta}$ by setting $\theta \in [0, \frac{\pi}{2}]$ with interval of $\frac{\pi}{20}$, and then use $M = 2\times10^4$ measurements in shadow estimation on each $\rho_{\mathrm{GHZ}_\theta}$ to bound the coherent information $I(A\rangle B)$ of $\rho_{\mathrm{GHZ}_\theta}$. We consider the bipartition of $\rho_{\mathrm{GHZ}_\theta}$ with two subsystems A and B, where $A\cup B = \{1, 1', 2, 2'\}$ and $A\cap B = \varnothing$. Each subsystem contains $|A|$ and $|B|$ qubits, respectively. We consider three cases of $B = \{1\}$, $B = \{1, 1'\}$ and $B = \{1, 1', 2\}$. The unbiased estimator of purities $\mathcal{P}_{\rho_{\mathrm{GHZ}_\theta}}$ and $\mathcal{P}_{\rho_B}$ are constructed with $\{\hat{\rho}_{\mathrm{GHZ}_\theta}^{(m)}\}$ by [55]

$$\hat{\mathcal{P}}(\rho_{\mathrm{GHZ}_\theta}) = \frac{1}{M(M-1)}\sum_{m\neq m'}\mathrm{Tr}\left[\hat{\rho}_{\mathrm{GHZ}_\theta}^{(m)}\hat{\rho}_{\mathrm{GHZ}_\theta}^{(m')}\right] \tag{8}$$

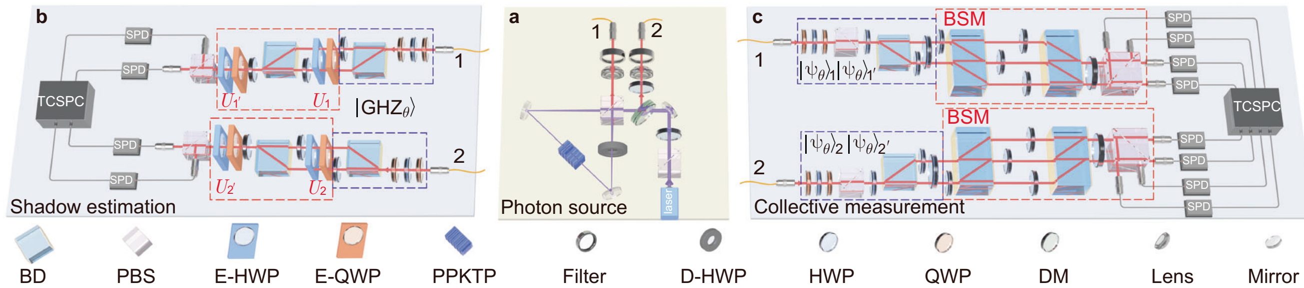

Fig. 1 | Schematic illustration of the experimental setup. a Generation of the biased polarization-entangled state $\cos\theta|HH\rangle_{12} + \sin\theta|VV\rangle_{12}$. **b** Setup to extend $\cos\theta|HH\rangle_{12} + \sin\theta|VV\rangle_{12}$ into $|\mathrm{GHZ}_\theta\rangle = \cos\theta|HhHh\rangle_{11'22'} + \sin\theta|VvVv\rangle_{11'22'}$, and demonstrate the shadow estimation scheme. **c** Setup to prepare two-copy states and implement the collective measurement scheme. Symbols used in **a**–**c** BD beam displacer, PBS polarization beam splitter, SPD single-photon detector, DM dichroic mirror, E-HWP electrically-rotated HWP, E-QWP electrically-rotated QWP, D-HWP dual-wavelength HWP, TCSPC time-correlated single-photon counting system. The abbreviation BSM represents Bell-state measurement.

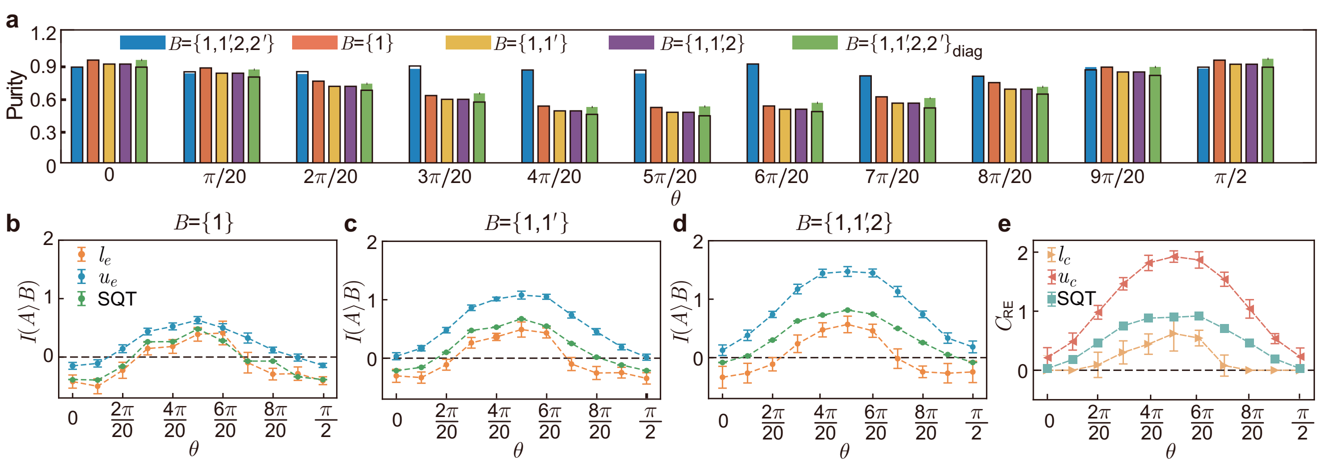

Fig. 2 | Experimental results of quantification of $I(A\rangle B)$ and C_{RE} on the prepared $\rho_{\mathrm{GHZ}_\theta}$ by shadow estimation. a The estimation of global purity $\hat{\mathcal{P}}(\rho_{\mathrm{GHZ}_\theta})$, marginal purity $\hat{\mathcal{P}}(\rho_B)$ and the purity of diagonal matrix $\hat{\mathcal{P}}(\rho_{\mathrm{GHZ}_{\theta,d}})$. The colored bars represent the results from shadow estimation, while the black frames represent the results from SQT for comparison. **b**–**d** The upper bound u_e and lower bound l_e of $I(A\rangle B)$ with $B=\{1\}$, $B=\{1,1'\}$ and $B=\{1,1',2\}$ respectively. **e** The upper bound u_c and lower bound l_c of $C_{\mathrm{RE}}(\rho_{\mathrm{GHZ}_\theta})$. The error bars represent the statistical error by repeating shadow estimation 10 times.

and

$$\hat{\mathcal{P}}(\rho_B) = \frac{1}{M(M-1)}\sum_{m\neq m'}\mathrm{Tr}\left[\hat{\rho}_B^{(m)}\hat{\rho}_B^{(m')}\right], \tag{9}$$

where $\hat{\rho}_B = \bigotimes_{n\in B} 3U_n^\dagger|b_n\rangle\langle b_n|U_n - \mathbb{I}_2$. The results of $\hat{\mathcal{P}}(\rho_{\mathrm{GHZ}_\theta})$ and $\hat{\mathcal{P}}(\rho_B)$ are shown in Fig. 2a. To indicate the accuracy of estimated purities, we perform standard quantum tomography (SQT)[64–66] on the prepared $\rho_{\mathrm{GHZ}_\theta}$ with 1.4×10^6 measurements, and treat the reconstructed state as target state. With the reconstructed $\rho_{\mathrm{GHZ}_\theta}$, we calculate the corresponding purities that are shown with black frames in Fig. 2a. The maximal error between purities (Eq. (8) and Eq. (9)) estimated from classical shadows and SQT is $\epsilon = 0.0132 \pm 0.0109$. The high accuracy ($\epsilon \ll 1$) agrees well with the theoretical prediction that the measurement cost of shadow tomography is in the order of $2^{|AB|}/\epsilon^2$ [33], while the SQT requires (at least) an order of $2^{|AB|}\mathrm{rank}(\rho_{AB})/\epsilon^2$ measurements to reach the same accuracy[67,68]. According to Eq. (3), the lower bound l_e and upper bound u_e of $I(A\rangle B)$ can be calculated with the estimated purities, and the results are shown with orange and blue dots in Fig. 2b–d, respectively. We observe that $l_e > 0$ with $\theta = \frac{3\pi}{20}, \frac{4\pi}{20}, \frac{5\pi}{20}$ and $\frac{6\pi}{20}$, which indicates the corresponding $\rho_{\mathrm{GHZ}_\theta}$ admits distillable entanglement. To investigate the tightness of lower and upper bounds of $I(A\rangle B)$, we calculate the $I(A\rangle B)$ with reconstructed $\rho_{\mathrm{GHZ}_\theta}$ instead of theoretical predictions as $I(A\rangle B)$ is sensitive to noise (See Supplementary Note 2 for analyzations). The results of calculated $I(A\rangle B)$) are shown with green dots in Fig. 2b–d, in which we observe that $I(A\rangle B)$) is well bounded by l_e and u_e expect $\theta = 6\pi/20$ in Fig. 2b. Similar phenomena are also observed in Fig. 2a, where the estimation of $\hat{\mathcal{P}}(\rho_{\mathrm{GHZ}_{\theta,d}})$ (green bars) are larger than the results from SQT. There are two main reasons attributed to these discrepancies. The first one is that the randomized measurement and SQT are performed separately, i.e., they are not obtained from the same copies of prepared $\rho_{\mathrm{GHZ}_\theta}$. There are unavoidable noises such as the slight drifts of the mounts holding BDs, which would accordingly introduce errors in state preparation and detection. The second one is that we use maximal likelihood estimation (MLE) in SQT to return a physical state from collected data. MLE is a biased estimation that underestimates properties of unknown quantum state[69], while the shadow tomography we implemented is an unbiased estimation of purity[55].

To bound $C_{\mathrm{RE}}(\rho_{\mathrm{GHZ}_\theta})$, we calculate the purity of the diagonal matrix of ρ_{GHZ} by $\hat{\mathcal{P}}(\rho_{\mathrm{GHZ}_{\theta,d}}) = \sum_{i=1}^{16} d_i^2$ with d_i being the diagonal elements of $\hat{\rho}_{\mathrm{GHZ}_\theta} = \sum_{m=1}^{M}\hat{\rho}_{\mathrm{GHZ}_\theta}^{(m)}$. The results of $\hat{\mathcal{P}}(\rho_{\mathrm{GHZ}_{\theta,d}})$ are shown with green bars in Fig. 2a. Thus, u_c and l_c are deduced with estimated $\hat{\mathcal{P}}(\rho_{\mathrm{GHZ}_{\theta,d}})$ and $\hat{\mathcal{P}}(\rho_{\mathrm{GHZ}_\theta})$ according to Eq. (6). As $C_{\mathrm{RE}} \geq 0$, we set $l_c = 0$ whenever it takes negative values. The results of the calculated u_c and l_c are shown with red and yellow triangles in Fig. 2e, in which one observes they tightly bound $C_{\mathrm{RE}}(\rho_{\mathrm{GHZ}_\theta})$ from SQT (cyan squares).

Detecting purity with collective measurements

The purity of a quantum state ρ can be indicated from two copies of ρ by $\mathcal{P}(\rho) = \mathrm{Tr}(\rho^2) = \mathrm{Tr}(\mathbb{V}\rho\otimes\rho)$ with $\mathbb{V}$ being the swap operation on

$\rho\otimes\rho$[70–73]. The purity from collective measurement has been demonstrated to extract Renyi entropy for violation of entropic inequalities to witness entanglement[70]. This Renyi quantity, while able to certify entanglement as it is an entanglement witness[74], does not quantify it. We consider the case of two-qubit state in the form of $|\psi_{2,\theta}\rangle = |\psi_\theta\rangle_1|\psi_\theta\rangle_2$ with $|\psi_\theta\rangle_1 = |\psi_\theta\rangle_2 = \cos\theta|0\rangle + \sin\theta|1\rangle$. Experimentally, $|\psi_{2,\theta}\rangle$ is encoded in the polarization DOF and the setup to generate $|\psi_{2,\theta}\rangle$ as shown in Fig. 1c. We first post-select the component $|H\rangle_1|H\rangle_2$ using two polarizing beam splitters (PBSs). By applying a HWP that transforms $|H\rangle$ to $\cos\theta|H\rangle + \sin\theta|V\rangle$ individually on photon 1 and photon 2, $|\psi_{2,\theta}\rangle$ is obtained. The copy of $|\psi_{2,\theta}\rangle$ is encoded in the path DOF, i.e., $|\psi_\theta\rangle_{1'} = |\psi_\theta\rangle_{2'} = \cos\theta|h\rangle + \sin\theta|v\rangle$.

The swap operation on $\mathbb{V}$ on $\rho\otimes\rho$ can be implemented by performing Bell-state measurement (BSM) between each qubit and its corresponding copy[36,75,76]. In our case, the BSM is performed between the polarization-encoded qubit 1(2) and the path-encoded qubit $1'(2')$[77], respectively. The outcome probability of the two BSMs on $\rho_{12}\otimes\rho_{1'2'}$ is denoted by $p_{ij} = \mathrm{Tr}[(\Pi_i\otimes\Pi_j)\rho_{\psi_{2,\theta}}\otimes\rho_{\psi_{2,\theta}}]$, where $\Pi_1 = |\Psi^+\rangle\langle\Psi^+|$, $\Pi_2 = |\Psi^-\rangle\langle\Psi^-|$, $\Pi_3 = |\Phi^+\rangle\langle\Phi^+|$, and $\Pi_4 = |\Phi^-\rangle\langle\Phi^-|$ are projectors onto Bell states $|\Psi^\pm\rangle = (|Hv\rangle \pm |Vh\rangle)/\sqrt{2}$ and $|\Phi^\pm\rangle = (|Hh\rangle \pm |Vv\rangle)/\sqrt{2}$. The purity of $\rho_{\psi_{2,\theta}}$ and the subsystem purity of $\rho_{\psi_{2,\theta,B}}$ with $B = \{2\}$ are then obtained by

$$\mathcal{P}(\rho_{\psi_{2,\theta}}) = 1 - 2(p_{12} + p_{32} + p_{42} + p_{21} + p_{23} + p_{24}), \tag{10}$$

and

$$\mathcal{P}(\rho_{\psi_{2,\theta,B}}) = 1 - 2(p_{12} + p_{22} + p_{32} + p_{42}). \tag{11}$$

Similarly, the purity of the diagonal matrix of $\rho_{\psi_{2,\theta}}$ can be obtained by

$$\mathcal{P}(\rho_{\psi_{2,\theta,d}}) = 1 - 2p_{33} + 2p_{44} - p_{11}. \tag{12}$$

The results of $\mathcal{P}(\rho_{\psi_{2,\theta}})$, $\mathcal{P}(\rho_{\psi_{2,\theta,B}})$ and $\mathcal{P}(\rho_{\psi_{2,\theta,d}})$ are shown in Fig. 3a, with $\theta\in[0,\frac{\pi}{2}]$ with interval of $\frac{\pi}{20}$. The lower bound l_e and upper bound u_e of $I(A\rangle B)$ are calculated according to Eq. (3) and shown in Fig. 3b. We observe $u_e < 0$ for all $\rho_{\psi_{2,\theta}}$, which indicates the prepared $\rho_{\psi_{2,\theta}}$ is less useful for entanglement distillation. Similarly, the lower bound l_c and upper bound u_c of $C_{\mathrm{RE}}(\rho_{\psi_{2,\theta}})$ can be calculated according to Eq. (6). The results are shown in Fig. 3c. Note that l_c is much closer to u_c compared to the case in Fig. 2e. This is because the bounds l_c and u_c are functions of the leading order term (purity) in Taylor expansion of the von Neumann entropy about pure states, so that l_c and u_c are tight for pure states. Experimentally, the prepared ρ_{12} and $\rho_{1'2'}$ are quite close to the ideal form of $|\psi_{2,\theta}\rangle$, while $\rho_{\mathrm{GHZ}_\theta}$ is much more noisy. The high accuracy of l_c and u_c is also confirmed by $C_{\mathrm{RE}}(\rho_{12})$ with reconstructed ρ_{12} from SQT, which is shown with cyan dots in Fig. 3c.

Discussion

We demonstrated universal and computable theoretical bounds to operationally meaningful measures of entanglement and coherence in terms of purity functionals. Then, we experimentally extracted these bounds by implementing two purity detection methods: shadow estimation and collective measurements. The experiment showed that quantum resources can be estimated, rather than just witnessed, with a precision that does not scale with the rank of the state (guaranteed by theory[33,55,67,68]), conversely to state tomography. The scalability of the measurement network makes purity detection employable in testing the successful preparation of quantum superpositions in large computational registers, certifying that a complex device has run a truly quantum computation. The proposed bounds are sufficiently tight for practically useful quantum states, i.e., the high-fidelity GHZ-like states or maximally coherent states, which are important entanglement and coherence resources that are widely used in quantum information protocols. The bounds Eqs. (2) and (5) represent the leading order term in Taylor's expansion of the von Neumann entropy. Thus, tightened bounds for noisy states can be extracted by evaluating the higher-order terms $\mathrm{Tr}(\rho^3), \mathrm{Tr}(\rho^4), \ldots, \mathrm{Tr}(\rho^d)$, which can be efficiently detected with hybrid shadow estimation[78,79]. In particular, the bounds become strict when we include moments of the system dimension. It would be interesting for future work to study the tightness of the bounds for the intermediate cases. Another unexplored direction is that one can extend the method proposed here to determine directly measurable bounds to the total correlations in multipartite systems $\{A_i\}$. For instance, consider the quantum analog of the multi-information between random variables[80,81]

$$\mathcal{I}(\rho_{A_1,\ldots,A_n}) = \min_{\bigotimes_i \sigma_{A_i}} S\left(\rho_{A_1,\ldots,A_n} || \bigotimes_i \sigma_{A_i}\right). \tag{13}$$

It is easy to verify that the product of the state marginals $\bigotimes_i \rho_{A_i}$ solves the minimization, $\mathcal{I}(\rho_{A_1,\ldots,A_n}) = \sum_i S(\rho_{A_i}) - S(\rho_{A_1,\ldots,A_n})$. Quantitative bounds to the total system correlations in terms of purities are given by a straightforward generalization of Eq. (2).

Our work has important and wide practical applications in various fields in quantum computation, communication, quantum thermodynamics, quantum many-body physics, etc. The proposed method has an immediate application in benchmarking current and near-term quantum technologies and serves as a basic and useful tool for analyzing and optimizing practical implementations of quantum information protocols.

Methods

Biased polarization-entangled photon source

We use a continuous-wave laser operating at a central wavelength of 405 nm with a full width at half maximum (FWHM) of 0.012 nm as our pump light source. The pump light passes through a PBS followed by an HWP set at $\theta/2$, which transforms the polarization of the pump light into $\cos\theta|H\rangle_p + \sin\theta|V\rangle_p$. The pump light passes PBS that transmits the component of $|H\rangle$ and reflects the component of $|V\rangle$. Then, the PPKTP crystal is coherently pumped from anticlockwise and clockwise directions, respectively, and the generated photons are superposed on the PBS, leading to the outcome state of $\cos\theta|HV\rangle_{12} + \sin\theta|VH\rangle_{12}$. An HWP set at 45° is

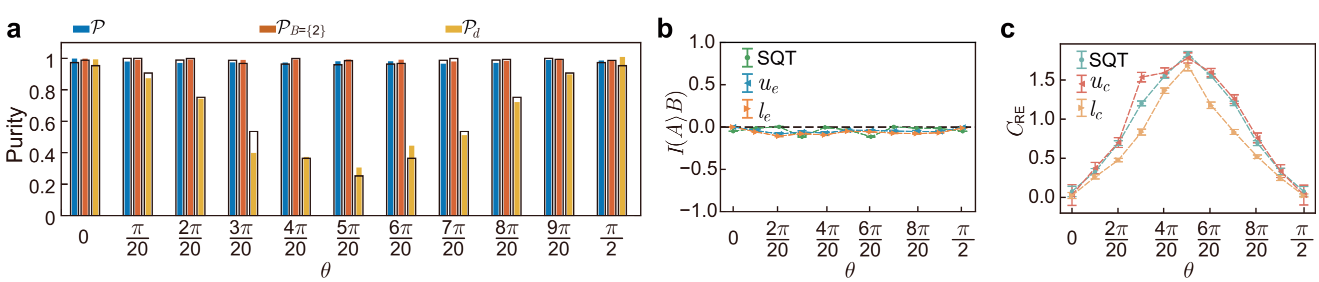

Fig. 3 | Experimental results of quantification of $I(A\rangle B)$ and C_{RE} of $\rho_{\psi_{2,\theta}}$ by collective measurements. a The estimated purities of $\mathcal{P}(\rho_{\psi_{2,\theta}})$, $\mathcal{P}(\rho_{\psi_{2,\theta,B}})$ and $\mathcal{P}(\rho_{\psi_{2,\theta,d}})$. **b** The upper bound u_e and lower bound l_e of $I(A\rangle B)$ with $B = \{2\}$. **c** The upper bound u_c and lower bound l_c of $C_{\mathrm{RE}}(\rho_{\psi_{2,\theta}})$. The error bars represent standard deviations obtained from conducting the experiment ten times.

applied on photon 2, which leads to a biased polarization-entangled state in form of $\cos\theta|HH\rangle_{12} + \sin\theta|VV\rangle_{12}$. To enhance collective efficiency, we employ lens L1 with a focal length of 200 mm and lens L2 with a focal length of 250 mm. The two photons pass through narrowband filters (NBFs) with an FWHM of 3 nm and then are coupled into single-mode fibers.

Shadow tomography

In shadow tomography, local random unitary operations $U_n \in \mathrm{Cl}_2$ are individually applied on each qubit of an N-qubit state ρ, where Cl_2 is the single-qubit Clifford group. Then the rotated state is measured on the Pauli-Z basis, producing a bit string $|b\rangle = |b_1 b_2 \cdots b_N\rangle$, $b_n \in \{0, 1\}$. The classical shadow of a single experimental run is constructed by $\hat{\rho} = \bigotimes_{n=1}^{N} 3U_n^{\dagger}|b_n\rangle\langle b_n|U_n - \mathbb{I}_2$ with $\mathbb{I}_2$ being identity matrix. By repeating the measurement M times, one has a collection of classical shadows $\{\hat{\rho}^{(m)}\}$ which is further exploited for the estimation of various properties of the underlying state ρ[30,33]. The random unitary operations $U_n \in \mathrm{Cl}_2$ on the polarization and path DOF are implemented with a combination of electrical-controlled half waveplate and quarter waveplate[57], and the projective measurements on the Pauli-Z basis are sequentially performed on the polarization and path DOF (See Supplementary Note 2 for more details).

Data availability

The data that support the findings of this study have been deposited in the Zenodo database with the identifier https://zenodo.org/records/11386676.

Code availability

The code supporting the findings of this study has been deposited in the Zenodo database with the identifier https://zenodo.org/records/11386676.

Received: 7 January 2024; Accepted: 30 May 2024;
Published online: 15 June 2024

References

1. Nielsen, M. A. & Chuang, I. L. Quantum computation and quantum information: 10th anniversary edition. *In: Cambridge University Press*. https://doi.org/10.1017/CBO9780511976667 (2010).
2. Bennett, C. H. & Wiesner, S. J. Communication via one- and two-particle operators on einstein-podolsky-rosen states. *Phys. Rev. Lett.* **69**, 2881–2884 (1992).
3. Ekert, A. K. Quantum cryptography based on bell's theorem. *Phys. Rev. Lett.* **67**, 661–663 (1991).
4. Bennett, C. H. et al. Teleporting an unknown quantum state via dual classical and einstein-podolsky-rosen channels. *Phys. Rev. Lett.* **70**, 1895–1899 (1993).
5. Horodecki, R., Horodecki, P., Horodecki, M. & Horodecki, K. Quantum entanglement. *Rev. Mod. Phys.* **81**, 865–942 (2009).
6. Streltsov, A., Adesso, G. & Plenio, M. B. Colloquium: quantum coherence as a resource. *Rev. Mod. Phys.* **89**, 041003 (2017).
7. Giovannetti, V., Lloyd, S. & Maccone, L. Advances in quantum metrology. *Nat. Photonics* **5**, 222–229 (2011).
8. Zhang, C. et al. Demonstrating quantum coherence and metrology that is resilient to transversal noise. *Phys. Rev. Lett.* **123**, 180504 (2019).
9. Åberg, J. Catalytic coherence. *Phys. Rev. Lett.* **113**, 150402 (2014).
10. Lostaglio, M., Jennings, D. & Rudolph, T. Description of quantum coherence in thermodynamic processes requires constraints beyond free energy. *Nat. Commun.* **6**, 6383 (2015).
11. Narasimhachar, V. & Gour, G. Low-temperature thermodynamics with quantum coherence. *Nat. Commun.* **6**, 7689 (2015).
12. Romero, E. et al. Quantum coherence in photosynthesis for efficient solar-energy conversion. *Nat. Phys.* **10**, 676–682 (2014).
13. Huelga, S. & Plenio, M. Vibrations, quanta and biology. *Contemp. Phys.* **54**, 181–207 (2013).
14. Lloyd, S. Quantum coherence in biological systems. *J. Phys. Conf. Ser.* **302**, 012037 (2011).
15. Lambert, N. et al. Quantum biology. *Nat. Phys.* **9**, 10–18 (2013).
16. Vidal, G. & Werner, R. F. Computable measure of entanglement. *Phys. Rev. A* **65**, 032314 (2002).
17. Hayden, P. M., Horodecki, M. & Terhal, B. M. The asymptotic entanglement cost of preparing a quantum state. *J. Phys. A: Math. Gen.* **34**, 6891 (2001).
18. Gühne, O. & Tóth, G. Entanglement detection. *Phys. Rep.* **474**, 1–75 (2009).
19. Bennett, C. H., DiVincenzo, D. P., Smolin, J. A. & Wootters, W. K. Mixed-state entanglement and quantum error correction. *Phys. Rev. A* **54**, 3824–3851 (1996).
20. Wootters, W. K. Entanglement of formation of an arbitrary state of two qubits. *Phys. Rev. Lett.* **80**, 2245–2248 (1998).
21. Schumacher, B. Quantum coding. *Phys. Rev. A* **51**, 2738–2747 (1995).
22. Brandão, F. G. S. L., Horodecki, M., Oppenheim, J., Renes, J. M. & Spekkens, R. W. Resource theory of quantum states out of thermal equilibrium. *Phys. Rev. Lett.* **111**, 250404 (2013).
23. ur Rehman, J., Hong, S., Kim, Y.-S. & Shin, H. Variational estimation of capacity bounds for quantum channels. *Phys. Rev. A* **105**, 032616 (2022).
24. Kitaev, A. & Preskill, J. Topological entanglement entropy. *Phys. Rev. Lett.* **96**, 110404 (2006).
25. Furukawa, S. & Misguich, G. Topological entanglement entropy in the quantum dimer model on the triangular lattice. *Phys. Rev. B* **75**, 214407 (2007).
26. Satzinger, K. J. et al. Realizing topologically ordered states on a quantum processor. *Science* **374**, 1237–1241 (2021).
27. Alba, V., Haque, M. & Läuchli, A. M. Entanglement spectrum of the two-dimensional bose-hubbard model. *Phys. Rev. Lett.* **110**, 260403 (2013).
28. Gerster, M. et al. Superfluid density and quasi-long-range order in the one-dimensional disordered bose–hubbard model. *New J. Phys.* **18**, 015015 (2016).
29. Laflorencie, N. Quantum entanglement in condensed matter systems. *Phys. Rep.* **646**, 1–59 (2016).
30. Brydges, T. et al. Probing rényi entanglement entropy via randomized measurements. *Science* **364**, 260–263 (2019).
31. Elben, A., Vermersch, B., Roos, C. F. & Zoller, P. Statistical correlations between locally randomized measurements: a toolbox for probing entanglement in many-body quantum states. *Phys. Rev. A* **99**, 052323 (2019).
32. Elben, A. et al. The randomized measurement toolbox. *Nat. Rev. Phys.* **5**, 9–24 (2023).
33. Elben, A. et al. Mixed-state entanglement from local randomized measurements. *Phys. Rev. Lett.* **125**, 200501 (2020).
34. Massar, S. & Popescu, S. Optimal extraction of information from finite quantum ensembles. *Phys. Rev. Lett.* **74**, 1259–1263 (1995).
35. Tarrach, R. & Vidal, G. Universality of optimal measurements. *Phys. Rev. A* **60**, R3339–R3342 (1999).
36. Islam, R. et al. Measuring entanglement entropy in a quantum many-body system. *Nature* **528**, 77–83 (2015).
37. Bagan, E., Ballester, M. A., Gill, R. D., Muñoz Tapia, R. & Romero-Isart, O. Separable measurement estimation of density matrices and its fidelity gap with collective protocols. *Phys. Rev. Lett.* **97**, 130501 (2006).

38. Wu, K.-D. et al. Experimental progress on quantum coherence: detection, quantification, and manipulation. *Adv. Quantum Technol.* **4**, 2100040 (2021).
39. Zhang, C. et al. Detecting metrologically useful asymmetry and entanglement by a few local measurements. *Phys. Rev. A* **96**, 042327 (2017).
40. Mandal, S. et al. Characterizing coherence with quantum observables. *Phys. Rev. Res.* **2**, 013157 (2020).
41. Huang, Y.et al. Measuring quantum entanglement from local information by machine learning. Preprint at https://doi.org/10.48550/arXiv.2209.08501 (2022).
42. Schumacher, B. & Nielsen, M. A. Quantum data processing and error correction. *Phys. Rev. A* **54**, 2629–2635 (1996).
43. Lloyd, S. Capacity of the noisy quantum channel. *Phys. Rev. A* **55**, 1613–1622 (1997).
44. Devetak, I. The private classical capacity and quantum capacity of a quantum channel. *IEEE Trans. Inf. Theory* **51**, 44–55 (2005).
45. Horodecki, M., Oppenheim, J. & Winter, A. Partial quantum information. *Nature* **436**, 673–676 (2005).
46. Bergh, B. & Gärttner, M. Entanglement detection in quantum many-body systems using entropic uncertainty relations. *Phys. Rev. A* **103**, 052412 (2021).
47. Friis, N., Vitagliano, G., Malik, M. & Huber, M. Entanglement certification from theory to experiment. *Nat. Rev. Phys.* **1**, 72–87 (2019).
48. Winter, A. & Yang, D. Operational resource theory of coherence. *Phys. Rev. Lett.* **116**, 120404 (2016).
49. Zhao, Q., Liu, Y., Yuan, X., Chitambar, E. & Winter, A. One-shot coherence distillation: towards completing the picture. *IEEE Trans. Inf. Theory* **65**, 6441–6453 (2019).
50. Ding, Q.-M., Fang, X.-X., Yuan, X., Zhang, T. & Lu, H. Efficient estimation of multipartite quantum coherence. *Phys. Rev. Res.* **3**, 023228 (2021).
51. Ren, H., Lin, A., He, S. & Hu, X. Quantitative coherence witness for finite dimensional states. *Ann. Phys.* **387**, 281–289 (2017).
52. Cincio, L., Subaşı, Y., Sornborger, A. T. & Coles, P. J. Learning the quantum algorithm for state overlap. *New J. Phys.* **20**, 113022 (2018).
53. Hou, Z. et al. Deterministic realization of collective measurements via photonic quantum walks. *Nat. Commun.* **9**, 1414 (2018).
54. Wu, K.-D. et al. Experimentally reducing the quantum measurement back action in work distributions by a collective measurement. *Sci. Adv.* **5**, eaav4944 (2019).
55. Huang, H.-Y., Kueng, R. & Preskill, J. Predicting many properties of a quantum system from very few measurements. *Nat. Phys.* **16**, 1050–1057 (2020).
56. Aaronson, S. Shadow tomography of quantum states. *In STOC'18-Proc.50th Annual ACM SIGACT Symposium on Theory of Computing*, 325–338 https://doi.org/10.1145/3188745.3188802 (ACM, 2018).
57. Zhang, T. et al. Experimental quantum state measurement with classical shadows. *Phys. Rev. Lett.* **127**, 200501 (2021).
58. Daley, A. J., Pichler, H., Schachenmayer, J. & Zoller, P. Measuring entanglement growth in quench dynamics of bosons in an optical lattice. *Phys. Rev. Lett.* **109**, 020505 (2012).
59. Życzkowski, K. Rényi extrapolation of shannon entropy. *Open Syst. Inf. Dyn.* **10**, 297–310 (2003).
60. Baumgratz, T., Cramer, M. & Plenio, M. B. Quantifying coherence. *Phys. Rev. Lett.* **113**, 140401 (2014).
61. Herbut, F. A quantum measure of coherence and incompatibility. *J. Phys. A Math. Theor.* **38**, 2959 (2005).
62. Chen, S., Yu, W., Zeng, P. & Flammia, S. T. Robust shadow estimation. *PRX Quant.* **2**, 030348 (2021).
63. Struchalin, G., Zagorovskii, Y. A., Kovlakov, E., Straupe, S. & Kulik, S. Experimental estimation of quantum state properties from classical shadows. *PRX Quant.* **2**, 010307 (2021).
64. Vogel, K. & Risken, H. Determination of quasiprobability distributions in terms of probability distributions for the rotated quadrature phase. *Phys. Rev. A* **40**, 2847–2849 (1989).
65. Leonhardt, U. Quantum-state tomography and discrete wigner function. *Phys. Rev. Lett.* **74**, 4101–4105 (1995).
66. White, A. G., James, D. F. V., Eberhard, P. H. & Kwiat, P. G. Nonmaximally entangled states: production, characterization, and utilization. *Phys. Rev. Lett.* **83**, 3103–3107 (1999).
67. Haah, J., Harrow, A. W., Ji, Z., Wu, X. & Yu, N. Sample-optimal tomography of quantum states. *IEEE Trans. Inf. Theory* **63**, 5628–5641 (2017).
68. O'Donnell, R. & Wright, J. Efficient quantum tomography. In *STOC'16-Proc. 48th Annual ACM SIGACT Symposium on Theory of Computing,* 899–912 https://doi.org/10.1145/2897518.2897544 (ACM 2016).
69. Schwemmer, C. et al. Systematic errors in current quantum state tomography tools. *Phys. Rev. Lett.* **114**, 080403 (2015).
70. Bovino, F. A. et al. Direct measurement of nonlinear properties of bipartite quantum states. *Phys. Rev. Lett.* **95**, 240407 (2005).
71. Yuan, Y. et al. Direct estimation of quantum coherence by collective measurements. *npj Quant. Inf.* **6**, 46 (2020).
72. Roik, J., Bartkiewicz, K., Černoch, A. & Lemr, K. Entanglement quantification from collective measurements processed by machine learning. *Phys. Lett. A* **446**, 128270 (2022).
73. Conlon, L. O. et al. Approaching optimal entangling collective measurements on quantum computing platforms. *Nat. Phys.* **19**, 351–357 (2023).
74. Terhal, B. M. Bell inequalities and the separability criterion. *Phys. Lett. A* **271**, 319–326 (2000).
75. Moura Alves, C. & Jaksch, D. Multipartite entanglement detection in bosons. *Phys. Rev. Lett.* **93**, 110501 (2004).
76. Girolami, D. Observable measure of quantum coherence in finite dimensional systems. *Phys. Rev. Lett.* **113**, 170401 (2014).
77. Li, J.-Y. et al. Activating hidden teleportation power: theory and experiment. *Phys. Rev. Res.* **3**, 023045 (2021).
78. Zhou, Y. & Liu, Z. A hybrid framework for estimating nonlinear functions of quantum states. Preprint at https://doi.org/10.48550/arXiv.2208.08416 (2022).
79. Peng, X.-J.et al. Experimental hybrid shadow tomography and distillation. Preprint at https://doi.org/10.48550/arXiv.2404.11850 (2024).
80. Han, T. S. Nonnegative entropy measures of multivariate symmetric correlations. *Inf. Control.* **36**, 133–156 (1978).
81. Modi, K., Paterek, T., Son, W., Vedral, V. & Williamson, M. Unified view of quantum and classical correlations. *Phys. Rev. Lett.* **104**, 080501 (2010).

Acknowledgements

The authors thank the anonymous reviewers for their insightful comments on the work. This work is supported by the National Key R&D Program of China (Grant no. 2019YFA0308200), the Innovation Program for Quantum Science and Technology (Grant no. 2023ZD0300200), the National Natural Science Foundation of China (Grants no. 11974213, no. 92065112, no. 12175003 and no. 12361161602), NSAF (Grant no. U2330201), Shandong Provincial Natural Science Foundation (Grants no. ZR2020JQ05 and no. ZR2023LLZ005), Taishan Scholar of Shandong Province (Grant no. tsqn202103013), Shenzhen Fundamental Research Program (Grant no. JCYJ20220530141013029), the Higher Education Discipline Innovation Project ("111") (Grant no. B13029) and the High-Performance Computing Platform of Peking University.

Author contributions

G.S., J.A.S., Q.Z., D.G., X.M., and X.Y. concreted the theory. H.L. conceived and designed the experiment. T.Z., L.L., X.-J.P., and H.L. carried out the experiment and analyzed data. All authors contributed to writing the manuscript.

Competing interests

The authors declare no competing interests.

Additional information

Supplementary information The online version contains supplementary material available at https://doi.org/10.1038/s41534-024-00857-2.

Correspondence and requests for materials should be addressed to Xiao Yuan or He Lu.

Reprints and permissions information is available at http://www.nature.com/reprints

Publisher's note Springer Nature remains neutral with regard to jurisdictional claims in published maps and institutional affiliations.